Chemical Engineering Journal 383 (2020) 123117

Contents lists available at ScienceDirect

Chemical Engineering Journal

journal homepage: www.elsevier.com/locate/cej

Constructing redox-active microporous hydrogen-bonded organic framework by imide-functionalization: Photochromism, electrochromism, and selective adsorption of C_2H_2 over CO_2

Li Wang[a,1], Lixiao Yang[a,1], Lele Gong[a,1], Rajamani Krishna[b], Zhi Gao[a], Yuan Tao[a], Wenhui Yin[a], Zhenzhen Xu[a], Feng Luo[a,*]

[a] State Key Laboratory of Nuclear Resources and Environment, School of Chemistry, Biology and Materials Science, East China University of Technology, Nanchang 330013, PR China

[b] Van't Hoff Institute for Molecular Sciences, University of Amsterdam, Science Park 904, 1098 XH Amsterdam, the Netherlands

HIGHLIGHTS

- A new multifunctional HOF (**ECUT-HOF-30**) was synthesized.
- **ECUT-HOF-30** exhibits excellent performance for C_2H_2/CO_2 separation.
- The photochromic and electrochromic properties of **ECUT-HOF-30** were observed.

GRAPHICAL ABSTRACT

We present a new concept of constructing redox-active microporous hydrogen-bonded organic framework (HOF) to modulate the electronic structure of this class of material for searching for new physical phenomenon and consequently advanced functions. The proof-of-concept results open up a gate for fundamental design of advanced HOFs with redox-active unit and versatility.

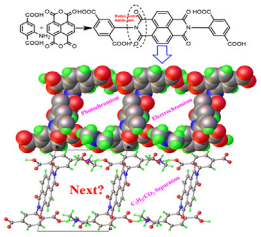

ARTICLE INFO

Keywords:
HOFs
Redox-active
Separation
Photochromism
Electrochromism

ABSTRACT

Hydrogen-bonded frameworks (HOFs) with permanent microporosity are still hard to obtain, due to the inherent nature of easy-to-collapse of HOF skeleton on solvent removal. On the other hand, tuning the electronic structure of HOFs by incorporating redox-active units for expanding the functionality of this class of material presents a waiting-for unveiled and highly desired field. In this work, the redox-active imide unit was utilized to construct HOF. The resultant HOF (namely **ECUT-HOF-30)** enables robust microporous structure of ca. 4.0 Å, performing effective separation of C_2H_2/CO_2 via the unique molecular recognition from imide oxygen atoms. Whilst exciting optoelectronic active properties such as photochromism and electrochromism were observed in this HOF. The proof-of-concept results open up a gate for fundamental design of advanced HOFs with redox-active unit and versatility.

1. Introduction

Porous materials built on light element such as C, H, N, O, B, typically presented by covalent organic frameworks (COFs) [1–3] and hydrogen-bonded organic frameworks (HOFs) [4–6] are recently receiving increasing attention due to their unique composition, structure,

* Corresponding author.
E-mail address: ecitluofeng@163.com (F. Luo).
[1] These authors contributed equally to this work.

https://doi.org/10.1016/j.cej.2019.123117
Received 20 July 2019; Received in revised form 5 October 2019; Accepted 8 October 2019
Available online 09 October 2019
1385-8947/

and promising applications in gas storage, gas separation, catalysis, and drug delivery. Different from the well-known porous platform of metal-organic frameworks (MOFs) which are connected by coordination interactions, COFs were principally synthetically directed by covalent interactions, while HOFs were constructed by non-covalent interactions involved in hydrogen bonds, π-π stacking, and van der Waals interactions. Accordingly, it is still extremely hard to obtain big single crystal to determine the structure of COFs by single crystal X-ray diffraction, consequently preventing us to have a precise insight into the structure-property relationships. By contrast, HOFs are usually highly crystalline materials and enable precise structural analysis. Nevertheless, this promising crystalline material are presently seriously restricted by their stability, which is typically reflected in this way that desolvation often causes the collapse of the frameworks of HOFs. Thereby, only a handful of successful cases have been reported to enable permanent porosity in the literature.

Especially, more effort needs to be devoted on the synthesis of microporous HOFs, as the narrow pore in HOFs would inherently seriously restrict the guest molecule and consequently prevent desolvation, finally leading to the collapse of HOF framework. Accordingly, in the literature HOFs with aperture size around 0.4 nm is still highly scarce (see Supporting information Table S1). It should be stressed here that, as revealed in recent advances, microporous MOFs with aperture size around 0.4 nm is found to well implement molecular sieving effect for separating some important industry-related molecules, for example, the dimensions of C_2H_2 and CO_2 are $0.33 \times 0.33 \times 0.57$ nm and $0.32 \times 0.33 \times 0.54$ nm, respectively. The cavity size of 0.4 nm matches well with the molecular size of these gases. Therefore, this class of materials presents a promising technique for generating high purity C_2H_2 or removing trace C_2H_2 molecule to avoid undesirable chemical reaction [7]. To this end, synthesizing HOFs with permanent microporosity around 0.4 nm is both scientific and industrial interesting.

On the other hand, the incorporation of redox-active unit into metal-organic frameworks (MOFs) and COFs is recently arousing extensive attention [8]. This is mainly because that this approach presents a very powerful tool to tune the electronic structure of MOFs and COFs, thus leading to enhanced performance or new physical properties. And a broad potential application in electrocatalysis, electrochromic devices, conductors, and switches has been established based on this class of material. However, to the best of our knowledge, the case of redox-active HOF is never documented until this work.

As shown in Scheme 1, we for the first time designed the imide-based H-type molecule to synthesize microporous HOF, based on these considerations as follows. (i) The big skeleton of this molecule facilitates to generate stable porous framework. (ii) Incorporation of redox-active component by imide-modification is expected to endow HOF with new physical properties such as photochromism and electrochromism, as imide unit can undergo single reversible one-electron reduction to form stable radical anions [9]. (iii) The imide unit can just act as H-bond acceptor, thus capable of selective recognition of some special molecule that can act as H-bond donor. As expected, the first redox-active microprous HOF of **ECUT-HOF-30** was obtained. And new physical phenomenon like that of photochromism and electrochromism, as well as selective adsorption of C_2H_2 over CO_2 was observed.

2. Experimental

2.1. Materials and instrumentation

The powder X-ray diffraction (PXRD) patterns were recorded on Bruker AXSD8 Discover powder diffractometer at 40 kV, 40 mA for Cu Kα, (λ = 1.5406 Å) at room temperature. Thermal gravimetric analysis (TGA) was performed using a TGA Q500 thermal analysis system from 30 to 800 °C under N_2 atmosphere at a constant rate of 10 °C/min. Infrared Spectra (IR) were measured by a Thermo Fisher ScientificNicolet iS5 spectrometer in the 500–4000 cm^{-1} region. The UV irradiation was carried out by MejiroGenossen MUV-165 (3.8 w/cm^2) with 365 nm filter. The UV–vis adsorption spectrum was obtained on a Hitachi UV-365 spectrophotometer. The gas sorption isotherms were collected on a Belsorp-max. Ultrahigh-purity-grade (> 99.999%) N_2, CO_2, and C_2H_2 gases were used in this adsorption measurement. To maintain the experimental temperatures liquid nitrogen (77 K) and temperature-programmed water bath (273 and 298 K) were used, respectively.

2.2. Synthesis of N,N,-bis(2-isophthalicacid)naphthalenediimide (H_4L)

The reagents and solvents were commercially available and were used without further purification. N,N,-bis(2-isophthalic acid)naphthalenediimide was synthesized according to the procedures in reference [10]. 10 mmol (2.68 g) 1,4,5,8-Naphthalenete-tracarboxylicdianhydride (NTCDA) was weighted in 250 ml round-bottom flask.

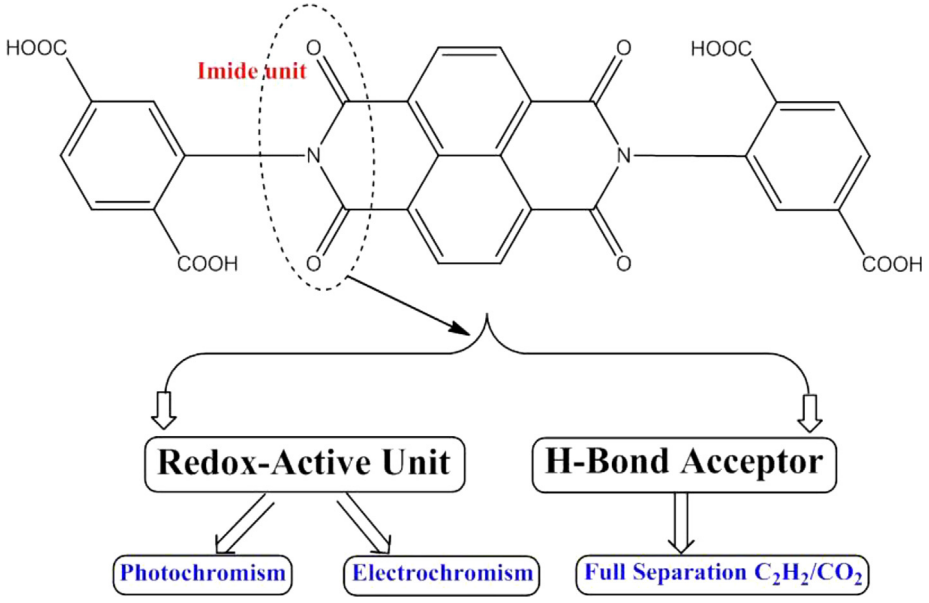

Scheme 1. The multi-carboxylate H-type molecule with redox-active imide unit designed in this work.

50 ml dried acetic acid was added and stirred for 10 min. Then 20 ml (3.62 g) 2-aminoterephthalic acid was added in the solution and allowed reflux at 119 °C. After 12 h, the reaction was cooled to room temperature and 100 ml deionized water was added. The product was washed by ethanol through filtration and dried in vacuum.

2.3. Synthesis of *ECUT-HOF-30*

10 mmol H_4L was solved in DMF solution with adding 300 µl 3 M/L HCl. The mixture were put into reaction still and then heated at 110 °C for 72 h with a ramp rate and cooling rate of 0.1 °C/min. The obtained single crystal was washed by DMF and dried at 50 °C.

2.4. Synthesis of *ECUT-HOF-30a*

The as-synthesized **ECUT-HOF-30** was exchanged with cyclohexane three times every day. After 3-day exchange, the products were evacuated under dynamic vacuum to obtain **ECUT-HOF-30a** for confirming the porosity.

2.5. Breakthrough experiments for C_2H_2/CO_2 gas mixture

The breakthrough experiments for C_2H_2/CO_2 were carried out at 298 K. About 0.72 g of activated **ECUT-HOF-30a** were filled in a column with 150 mm in length and 46 mm in diameter. At the beginning, the He flow through the column and then the C_2H_2/CO_2 mixture (50/50) passed through the column with 2 ml/min. The passed gas was detected by Hiden mass-spectrometer.

2.6. Density-functional theory calculations

A series of models for simulating the C_2H_2 and CO_2 gases adsorption in **ECUT-HOF-30** pores have been established. The optimization structures were performed by employing Density function theory (DFT) calculations, where the project-augmented wave (PAW) pseudopotentials and the Perdew-Burke-Ernzerhof (PBE) exchange-correlation functional were utilized, as implemented in the Vienna ab initio Simulation Package (VASP) code. The structures before and after adsorption were optimized aiming to the global energy minimum, fully relaxed until the residual force convergence value on each tom being less 0.01 eV/Å. The Brillouin zone was sampled by 3 × 3 × 1 Gamma k-point mesh and the wave functions were expanded using a plane-wave basis set with kinetic energy cutoff of 550 eV. Spin-polarization and van der Waals were considered in all calculations.

2.7. Crystallographic investigation

The data collection of single crystal was performed on a Bruker-AXS SMART Breeze CCD diffractometer using graphite monochromated Mo Kα radiation (λ = 0.71073 Å). The simulated powder patterns were calculated by Mercury 1.4. The crystal structure was solved and refined by SHELXTL program package.2.7.

The selected crystallographic data and refinement parameters for the single crystal are summarized in Table 1. CCDC1888690 for **ECUT-HOF-30** contains the supplementary crystallographic data for this paper. The cif file can be download free from the Cambridge Crystallographic Data Centre.

3. Results and discussion

3.1. Material synthesis and characterization

ECUT-HOF-30 was prepared using solvothermal technique by dissolving N,N,-bis(2-isophthalic acid)naphthalenediimide (H_4L) in DMF with the presence of HCl at 110 °C. The addition of HCl contributes to dissolve H_4L in DMF. The yield is up to 90%. The phase purity of the crystal samples is confirmed by powder X-ray diffraction (PXRD, Supporting information, Fig. S1).

Table 1
Crystal structure information for **ECUT-HOF-30**.

Compound	**ECUT-HOF-30**
Formula	$C_{20}H_{21}N_3O_7$
Formula weight	415.40
Color	Light yellow
Crystal system	triclinic
Space group	*P − 1*
a (Å)	8.4223(9)
b (Å)	9.6930(10)
C (Å)	12.7665(13)
α	78.488(9)
β	83.386(9)
γ	87.280(9)
Volume (Å^3)	1014.14
Z	2
Temperature for data collection (K)	293
Range for data collection θ(°)	0.997–25
No. of measured reflections	11,012
No. of unique reflections	3564
No. of parameters	279
No. of restraints	0
Goodness-of-fit on F^2	1.035
Final R indexes [I ≥ 2σ(I)]	R_1 = 0.0858,wR_2 = 0.2239
Final R indexes [all data]	R_1 = 0.1773, wR_2 = 0.2757

Single-crystal X-ray diffraction analysis at room temperature shows that **ECUT-HOF-30** crystallizes in the triclinic space group *P-1*, and exhibits a microporous hydrogen-bonded framework. One-dimensional rectangular channels of ca. 4.0 × 4.1 Å^2, occupied by free DMF molecules, are observed in the HOF along the crystallographic *a* axis (Fig. 1a and b). Notably, only very weak C—H···O supramolecular interactions between DMF molecules and HOF framework is observed, suggesting the possibility to obtain permanent porosity (Fig. S2). In the literature, several supramolecular synthons such as benzimidasolone, pyrazole, the 2,4-diaminotriazinyl group, and a dimer of carboxy groups have been successfully applied to construct of HOFs [4–6]. By contrast, in this HOF we observed two different H-bond modes, one being the single hydrogen bond between two adjacent carboxyl groups (O···O/2.53 Å, O—H···O/169.17°, Fig. 1c) and the other being the hydrogen bonds between $[NH_2(CH_3)_2]^+$ ions, in-situ formed from the decomposition of DMF, and two carboxylate oxygen atoms of H_2L^{2-}(N···O/2.92 Å and 2.71 Å, N—H···O/138.70° and 167.64°, Fig. 1d). For each H_2L^{2-} molecule, the middle naphthalene fragments located at the *b* axis show big distortion with the two terminal 1,4-benzenedicarboxylate proportion, giving a dihedral angel of ca. 83.5°, whilst the two 1,4-benzenedicarboxylate proportion are arranged in the parallel fashion.

3.2. Thermal gravimetric analysis

To generate porosity in **ECUT-HOF-30**, we first explored its thermostability by thermal gravimetric analysis (TGA) (Fig. S3). It shows that the guest solvent DMF molecules and dimethylamine ions are gradually released from room temperature to 290 °C. The loss of DMF solvent molecules can be finished before 180 °C (calc. 17.6%, exp. 17.6%). The following approximately 11% weight loss until 290 °C can be attributed to the released hydrogen-bonded dimethylamine ions. After 430 °C, significant weight loss was observed, which was corresponded to decomposition of framework. To confirm the stability of HOF framework after desolvation, temperature-variable PXRD test was performed. Apparently, the peak positions of all the diffraction are almost the same with as-synthesized **ECUT-HOF-30**. In other words, the HOF framework is well maintained even after loss of guest molecules (Fig. S1).

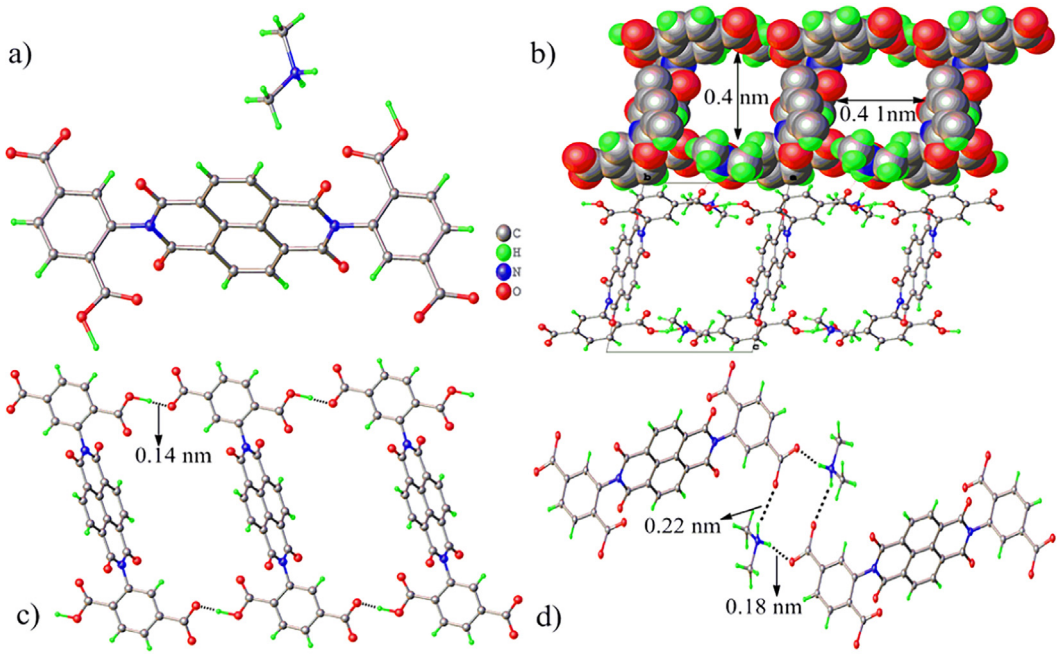

Fig. 1. The crystal structure of **ECUT-HOF-30**. a) The major composition of H_2L^{2-} and $[NH_2(CH_3)_2]^+$ fragments. b) View of the HOF framework formed by both hydrogen bonds and van der Waals interactions. The 1D pore with aperture around 0.4 nm along *a* axis is highlighted. c) View of the hydrogen bonds between two adjacent H_2L^{2-} molecules. d) View of the hydrogen bonds between H_2L^{2-} molecules and $[NH_2(CH_3)_2]^+$ ions.

3.3. Porosity measurement

In order to confirm the porosity, gas adsorption measurements were conducted on the activated samples (namely **ECUT-HOF-30a**), where the PXRD patterns of **ECUT-HOF-30a** agree well with the as-synthesized samples, suggesting the well-maintained HOF skeleton and potential porosity. N_2 was initially tested at 77 K (Fig. 2). However, only negligible N_2 uptake with linear adsorption profile was observed, which was previously reported to be a common phenomenon in the microporous HOFs [6]. Then we explored CO_2 adsorption at 196 K and moderate CO_2 uptake and reversible desorption behavior was observed, confirming the microporosity of **ECUT-HOF-30**. In terms of this result, the Langmuir surface area was estimated to be 402 m^2/g.

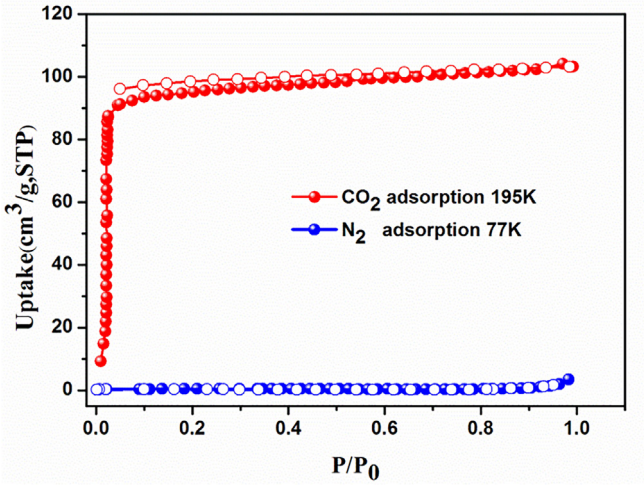

Fig. 2. N_2 and CO_2 gas adsorption isotherms for **ECUT-HOF-30a**. Filled symbols represent adsorption, while empty symbols represent desorption.

3.4. C_2H_2/CO_2 separation

The permanent porosity and suitable pore aperture size of **ECUT-HOF-30** encouraged us to further examine its application in gas storage and selective gas separation. The sorption isotherms of C_2H_2 and CO_2 were collected at 273 K and 296 K, respectively. As shown in Fig. 3, at 1 bar pressure, moderate C_2H_2 uptake of 53.8 cm^3/g at 273 K and 43.7 cm^3/g at 298 K, as well as low CO_2 uptake of 17 cm^3/g at 273 K and 9 cm^3/g at 298 K were observed. Note that the C_2H_2/CO_2 uptake ratio is up to 4.8-fold, presenting the highest value among the reported HOFs materials (see Table S2),[11] implying its promising potential in C_2H_2/CO_2 separation. The humidity stability of **ECUT-HOF-30a** was also checked (Fig. S4). The activated samples were exposed to air for 12 h, then the C_2H_2 adsorption was measured again. The similar C_2H_2 adsorption isotherm before and after exposure to air revealed that the structure of **ECUT-HOF-30a** was little affected by humidity.

To further explore the preferential adsorption mechanism, the isosteric heats of adsorption (Q_{st}) of C_2H_2 and CO_2 were calculated from the dual-site Langmuir-Freundlich model using the Clausius-Clapeyron equation [12]. It is well known that the higher Q_{st} indicates the stronger adsorption. As shown in Fig. 3, the value of Q_{st} for C_2H_2 is higher than that of CO_2. The Q_{st} of C_2H_2 is approximately 23.8 kJ/mol while for CO_2 is 21 kJ/mol, indicative of stronger interactions between HOF and C_2H_2 over HOF and CO_2. Furthermore, the C_2H_2/CO_2 adsorption selectivity (S) was estimated by the ideal adsorbed solution theory (IAST) calculations. Fig. 3 presents the IAST calculations of the component loading for C_2H_2 and CO_2 in equimolar mixture as a function of the total bulk gas-phase pressure at 298 K. As shown in Fig. 3, at 298 K, the C_2H_2/CO_2 selectivity of **ECUT-HOF-30a** gives $S = 9$ at 100 kPa. Generally speaking, material with $S > 8$ is viewed to be excellent separation materials [7], which further confirms its application in C_2H_2/CO_2 separation.

The transient breakthrough simulations of C_2H_2/CO_2 separation for a total gas at 100 kPa and 298 K was carried out. A typical breakthrough for 50/50 C_2H_2/CO_2 mixtures is shown in Fig. S5. A complete separation of C_2H_2/CO_2 is observed, also strongly supporting its superior application in C_2H_2/CO_2 separation. To further examined the

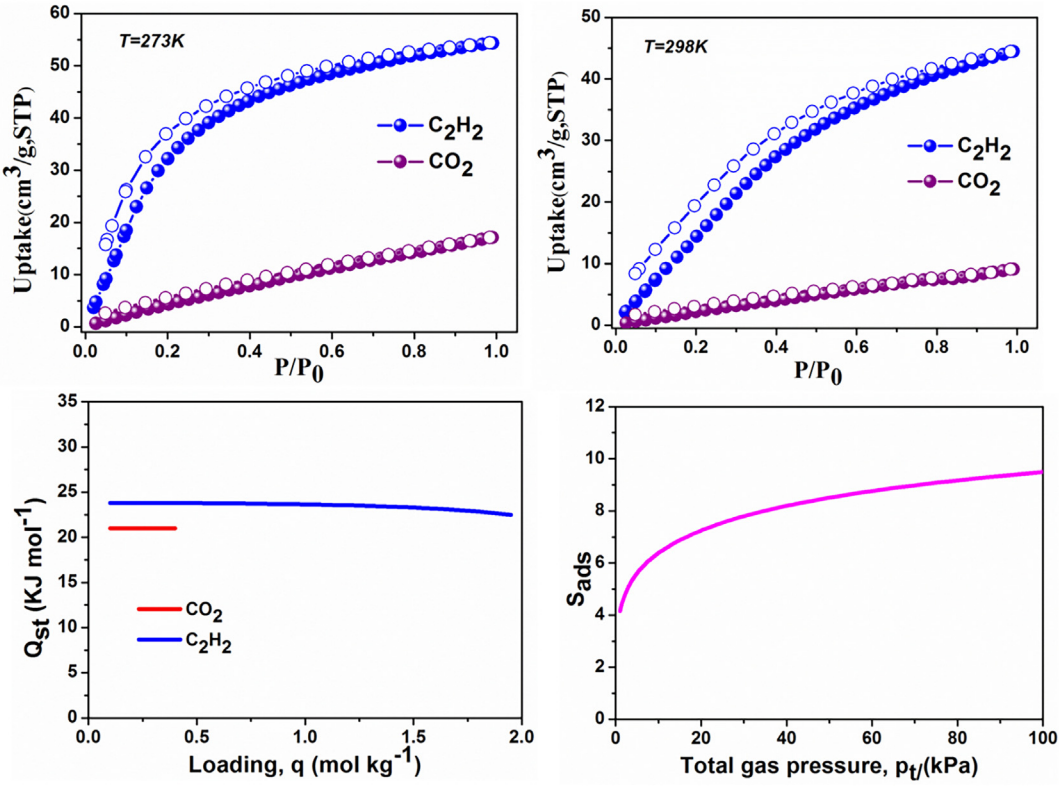

Fig. 3. The adsorption isotherms of C_2H_2 and CO_2 of **ECUT-HOF-30a** at 273 K (a) and 298 K (b). Filled symbols represent adsorption, while empty symbols represent desorption. The isosteric heat of adsorption for C_2H_2 and CO_2 in **ECUT-HOF-30a** (c) and IAST calculations of adsorption selectivity of **ECUT-HOF-30a** at 298 K with 50/50 C_2H_2/CO_2 mixture (d).

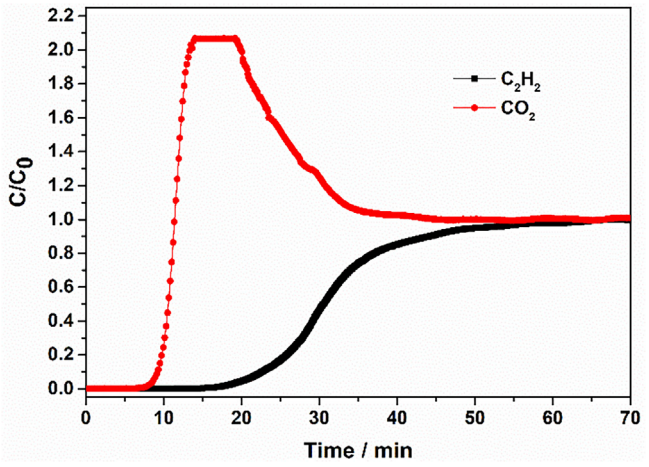

Fig. 4. Experimental column breakthrough curves for C_2H_2/CO_2 separations (50/50) with **ECUT-HOF-30a** at 298 K. The total flow is 2 ml/min.

adsorption processes of **ECUT-HOF-30a** in practical situation, the experimental breakthrough studies were also performed in equimolar gas mixture at 298 K. As shown in Fig. 4, the CO_2 was detected after the gas mixture flow into the column for about 9 min. However, the C_2H_2 was not passed through the column until ca. 20 min. Clearly, the separation of C_2H_2/CO_2 for **ECUT-HOF-30a** can be effectively achieved.

3.5. DFT calculation

To disclose the mechanism for such outstanding selective C_2H_2 adsorption over CO_2, the DFT (density functional theory) calculation was performed. As shown in Fig. 5, both C_2H_2 and CO_2 sit at the channels but with different gesture. In the C_2H_2- loaded optimal structure, the C_2H_2 molecules is lying horizontally to fulfill the 1D channel and shows strong hydrogen bonds with O···C distance of ca. 3.11 Å/3.05 Å and C—H···O angle of 148.29°/133.36° between imide oxygen atoms and C_2H_2 molecule, where, as expected, imide oxygen acts as H-bond acceptor and C_2H_2 molecule acts as H-bond donor. By contrast, in CO_2-loaded optimal structure, the CO_2 molecule is lying vertically with partial occupation of the 1D channel and shows no obvious supramolecular interactions with HOF skeleton. Thereby, the selective C_2H_2 adsorption over CO_2 is rationally realized, due to both the proper aperture size around 4.0 Å and recognized supramolecular interactions from HOF skeleton. Similar phenomenon was also observed in other materials for gas separation [13]. For example, FJU-22a can separate C_2H_2 from the C_2H_2/CO_2 mixture. The DFT calculation shows that the hydrogen-bonding interactions exist between C_2H_2 and the framework O of FJI-22a, while no interaction between CO_2 and FJU-22a was observed.

3.6. Photochromic and electrochromic properties

The successful of incorporation of imide unit into HOF encourages us to explore its redox-active properties. Firstly we examined the photochromic property. It is well known that molecules possessing photochromic properties have wide application in various productions of photochromic glasses, lenses, information storage and so on. Therefore, much work would be focused on introducing related functional groups such as diarylethenes and azobenzenes when designing and synthesizing materials. In our work, **ECUT-HOF-30** is the first example of functionalized HOF that displayed the photochromic property. **ECUT-HOF-30** was sensitive to UV light. Slight colour change from light-yellow to dark yellow was observed upon UV irradiation (365 nm) for three minutes (Fig. 6). And no detectable structural change was observed for the photochromic samples, relative to the pristine sample, as

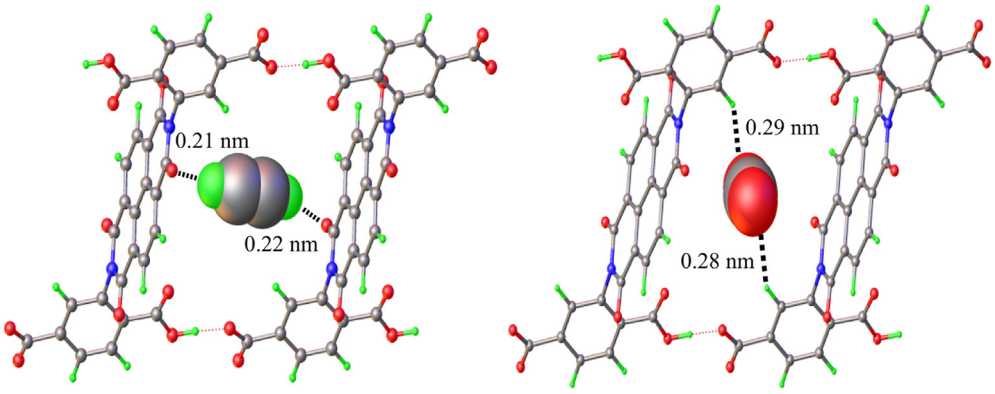

Fig. 5. The structure after loading the gas molecules in HOF-imide. left: C_2H_2, right: CO_2. The yellow, blue, red, and green are C, N, O and H, respectively, and the dotted line representing bonds between different atoms. (For interpretation of the references to color in this figure legend, the reader is referred to the web version of this article.)

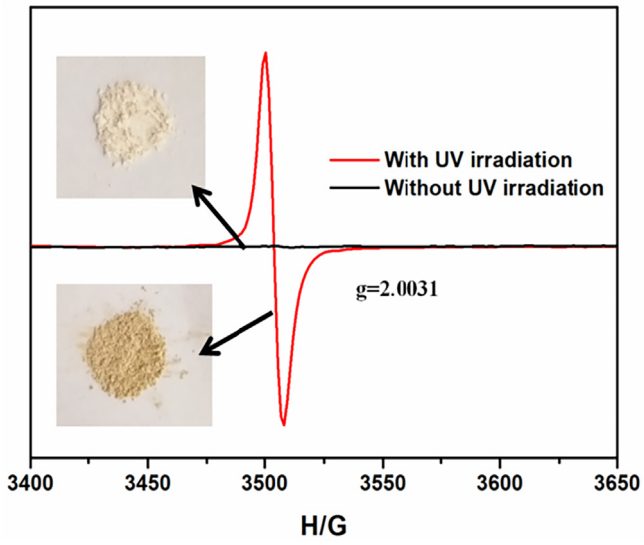

Fig. 6. ESR spectra of **ECUT-HOF-30** with and without UV irradiation.

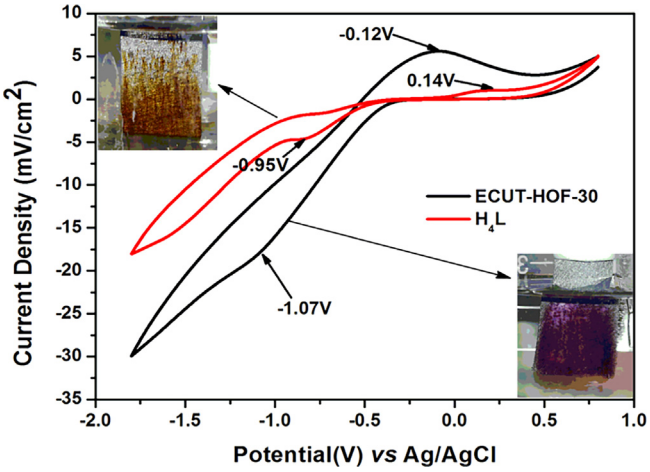

Fig. 7. A comparison of CV curves of **ECUT-HOF-30** and H_4L.

evidenced by their PXRD patterns and infrared spectrum results (Figs. S6 and S7). This is mainly because this type of photochromism is due to formation of free radical that usually does not cause obvious structure exchange [14]. To confirm this claim, the UV–vis spectrum of **ECUT-HOF-30** under UV irradiation with varied exposure time were tested and compared with the counterpart without UV. As shown in Fig. S8, a strong absorption band around 380 nm was found for all the curves, which was corresponded to the n-π* and π-π* transition of the aromatic carboxylate ligands. Remarkably, after irradiation for 5 min, several new additional peaks (604 nm, 690 nm, 780 nm) were generated, which arises from a photo-induced electron-transfer transition [9]. It is known that naphthalenediimide is redox-active and can generate radicals with irradiation. The formation of free radical for the samples after UV irradiation can be directly reflected by the electron spin resonance (ESR) spectra, where the formation of new signal at g = 2.0031 was observed for the samples after UV irradiation.

Next, the electrochromic function was monitored by cyclic voltammetry (CV, See Supporting Video) measurement. As shown in Fig. 6, the electrochromic test was carried out by loading **ECUT-HOF-30** on the carbon paper and then measured in water, using PBS buffer solution (PH = 7) as electrolyte. Interestingly, fast electrochromic behavior was observed, affording exquisite colour change from yellow to purple and one quasi-reversible one-electron reductions at $E_{pc} = -1.07$ V. As shown in Fig. 7, a comparison in CV curves was given for HOF material and H_4L. Both of them showed one broad reduction peak, which was corresponded to the formation of the radical anion $[H_2L^{2-}]^{\cdot -}$.[9] Notably, the H_4L molecule results in the colour change from white to deep yellow and one quasi-reversible one-electron reductions at $E_{pc} = -0.95$ V. Such difference in colour and reduction potential are mainly due to the immobilization of H_4L molecule in HOF or difference in the electrolyte diffusion limitations [9e]. To observe the spectral change of **ECUT-HOF-30** upon reduction, the UV–vis spectroelectrochemistry was employed. As shown in Fig. S9, at neutral state the color of **ECUT-HOF-30** was yellow and no obvious absorption band was found in the UV–vis spectrum from 400 to 800 nm. When the applied potential was set to −1.7 V, it exhibited fast colour change to dark purple. Meanwhile, the observation of new peak at 491 nm, 615 nm, and 745 nm is ascribed to be the formation of the radical anion of $[H_2L^{2-}]^{\cdot -}$ [9].

4. Conclusions

In conclusion, by anchoring imide unit we successfully synthesized the first redox-active HOF. Both the 0.4 nm microporous size of HOF framework and the H-bond-directing host-guest interactions derived from imide unit enable high C_2H_2 adsorption uptake, but very low CO_2 adsorption capacity, creating a ultrahigh C_2H_2/CO_2 ratio up to 4.8 times, implying full separation of C_2H_2/CO_2. Most importantly, this redox-active HOF also affords some new physical property such as photochromism and electrochromism, thus expanding the application of HOF in related fields. All the results show that redox-active HOFs are an interesting and promising subject worthy of further investigation for targeting multi-functional HOFs.

Declaration of Competing Interest

The authors declare that they have no known competing financial interests or personal relationships that could have appeared to

influence the work reported in this paper.

Acknowledgments

We thanks to the National Science Foundation of China (21871047 and 21661001), the Natural Science Foundation of Jiangxi Province of China (20181ACB20003), and the Doctoral Scientific Research Starting Foundation of East China University of Technology, Nanchang (DHBK2018044).

Appendix A. Supplementary data

Supplementary data to this article can be found online at https://doi.org/10.1016/j.cej.2019.123117.

References

[1] a) A.P. Côté, A.I. Benin, N.W. Ockwig, M. O'Keeffe, A.J. Matzger, O.M. Yaghi, Porous, crystalline, covalent organic frameworks, Science 310 (2005) 1166–1170;
b) E. Jin, M. Asada, Q. Xu, S. Dalapati, M.A. Addicoat, M.A. Brady, H. Xu, T. Nakamura, T. Heine, Q. Chen, D. Jiang, Two-dimensional sp2 carbon-conjugated covalent organic frameworks, Science 357 (2017) 673–676;
c) T. Ma, E.A. Kapustin, S.X. Yin, L. Liang, Z. Zhou, J. Niu, L.-H. Li, Y. Wang, J. Su, J. Li, X. Wang, W.D. Wang, W. Wang, J. Sun, O.M. Yaghi, Single-crystal x-ray diffraction structures of covalent organic frameworks, Science 361 (2018) 48–52.

[2] a) X. Han, J. Huang, C. Yuan, Y. Liu, Y. Cui, Covalent organic frameworks for high performance liquid chromatographic enantioseparation, J. Am. Chem. Soc. 140 (2018) 892–895;
b) S.L. José, J.M. María, Z. Félix, Covalent organic frameworks based on schiff-base chemistry: synthesis, properties and potential applications, Chem. Soc. Rev. 45 (2016) 5635–5671.

[3] a) Y.D. San, W. Wei, Covalent organic frameworks (COFs):from design to applications, Chem. Soc. Rev. 42 (2013) 548–568;
b) X. Feng, X. Ding, D. Jiang, Covalent organic frameworks, Chem. Soc. Rev. 41 (2012) 6010–6022.

[4] a) X.Z. Luo, X.J. Jia, J.H. Deng, J.L. Zhong, H.J. Liu, K.J. Wang, D.C. Zhong, A-microporous hydrogen-bonded organic framework: exceptional stability and highly selective adsorption of gas and liquid, J. Am. Chem. Soc. 135 (2013) 11684–11687;
b) L.J. Barbour, Crystal porosity and the burden of proof, Chem. Commun. 11 (2006) 1163–1168;
c) P. Sozzani, S. Bracco, A. Comotti, L. Ferretti, R. Simonutti, Methane and carbon dioxide storage in a porous van der Waals crystal, Angew. Chem. Int. Ed. 44 (2005) 1816–1820;
d) P. Sozzani, A. Comotti, R. Simonutti, T. Meersmann, J.W. Logan, A. Pines, A porous crystalline molecular solid explored by hyperpolarized xenon, Angew. Chem. Int. Ed. 39 (2000) 2695–2699;
e) A. Comotti, R. Simonutti, S. Stramare, P. Sozzani, 13C and 31P MAS NMR investigations of spirocyclotriphosphazene nanotubes, Nanotechnology 10 (1999) 70–76;
f) R.B. Lin, Y.B. He, P. Li, H.L. Wang, W. Zhou, B.L. Chen, Multifunctional porous hydrogen-bonded organic framework materials, Chem. Soc. Rev. 48 (2019) 1362–1389;
g) T.G. Carroll, C. Hunt, R. Garwick, G. Wu, R. Dobrovetsky, G. Ménard, An untethered C3v-symmetric triarylphosphine oxide locked by intermolecular hydrogen bonding, Chem. Commun. 55 (2019) 3761–3764;
h) G.L. Xing, I. Bassanetti, S. Bracco, M. Negroni, C. Bezuidenhout, T. Ben, P. Sozzani, A. Comotti, A double helix of opposite charges to form channels with unique CO2 selectivity and dynamics, Chem. Sci. 10 (2019) 730–736;
i) I. Hisaki, Y. Suzuki, E. Gomez, Q. Ji, N. Tohnai, T. Nakamura, A. Douhal, Acid responsive hydrogen-bonded organic frameworks, J. Am. Chem. Soc. 141 (2019) 2111–2121;
j) D. Meng, G.G. Liu, C.Y. Xiao, Y.J. Shi, L. Zhang, L. Jiang, K.K. Baldridge, Y. Li, J.S. Siegel, Z.H. Wang, Corannurylene pentapetalae, J. Am. Chem. Soc. 141 (2019) 5402–5408.

[5] a) W. Yang, A. Greenaway, X. Lin, R. Matsuda, A.J. Blake, C. Wilson, W. Lewis, P. Hubberstey, S. Kitagawa, N.R. Champness, M. Schröer, Exceptional thermal stability in a supramolecular organic framework: porosity and gas storage, J. Am. Chem. Soc. 132 (2010) 14457–111469;
b) M. Mastalerz, I.M. Oppel, Rational construction of an extrinsic porous molecular crystal with an extraordinary high specific surface area, Angew. Chem. Int. Ed. 51 (2012) 5252–5255;
c) K.J. Msayib, D. Book, P.M. Budd, N. Chaukura, K.D.M. Harris, M. Helliwell, S. Tedds, A. Walton, J.E. Warren, M. Xu, N.B. McKeown, Nitrogen and hydrogen adsorption by an organic microporous crystal, Angew. Chem. Int. Ed. 48 (2009) 3273–3277;
d) X.Z. Luo, X.J. Jia, J.H. Deng, J.L. Zhong, H.J. Liu, K.J. Wang, D.C. Zhong, Microporous hydrogen-bonded organic framework: exceptional stability and highly selective adsorption of gas and liquid, J. Am. Chem. Soc. 135 (2013) 11684–11687;
e) H. Wang, B. Li, H. Wu, T.L. Hu, Z. Yao, W. Zhou, S. Xiang, B. Chen, A flexible microporous hydrogen-bonded organic framework for gas sorption and separation, J. Am. Chem. Soc. 137 (2015) 9963–9970;
f) I. Hisaki, S. Nakagawa, N. Tohnai, M. Miyata, A C3-symmetric macrocycle-based, hydrogen-bonded, multiporous hexagonal network as a motif of porous molecular crystals, Angew. Chem. Int. Ed. 54 (2015) 3008–3012;
g) J. Lü, C. PereKrap, M. Suyetin, N.H. Alsmail, Y. Yan, S. Yang, W. Lewis, E. Bichoutskaia, C.C. Tang, A.J. Blake, R. Cao, M. Schröer, A robust binary supramolecular organic framework (SOF) with high CO2 adsorption and selectivity, J. Am. Chem. Soc. 136 (2014) 12828–12831;
h) K.D. Zhang, J. Tian, D. Hanifi, Y. Zhang, A.C.H. Sue, T.Y. Zhou, L. Zhang, X. Zhao, Y. Liu, Z.T. Li, Towards a single-layer two-dimensional honeycomb supramolecular organic framework in water, J. Am. Chem. Soc. 135 (2013) 17913–17918;
i) S.L. Cai, W.G. Zhang, R.N. Zuckermann, Z.T. Li, X. Zhao, Y. Liu, The organic flatland-recent advances in synthetic 2D organic layers, Adv. Mater. 27 (2015) 5762–5770;
j) R. Kubota, S. Tashiro, M. Shiro, M. Shionoya, In situ x-ray snapshot analysis of transient molecular adsorption in a crystalline channel, Nat. Chem. 6 (2014) 913–918.

[6] a) J. Lü, R. Cao, Porous organic molecular frameworks with extrinsic porosity: a platform for carbon storage and separation, Angew. Chem. Int. Ed. 55 (2016) 9474–9480;
b) A. Chaix, G. Mouchaham, A. Shkurenko, P. Hoang, B. Moosa, P.M. Bhatt, K. Adil, K.N. Salama, M. Eddaoudi, N.M. Khashab, Trianglamine-based supramolecular organic framework with permanent intrinsic porosity and tunable selectivity, J. Am. Chem. Soc. 140 (2018) 14571–14575;
c) Y.H. Luo, X.T. He, D.L. Hong, C. Chen, F.H. Chen, J. Jiao, L.H. Zhai, L.H. Guo, B.W. Sun, A dynamic 3D hydrogen-bonded organic frameworks with highly water affinity, Adv. Funct. Mater. 28 (2018) 1804822–1804828;
d) Y. Li, M. Handke, Y.S. Chen, A.G. Shtukenberg, C.T. Hu, M.D. Ward, Guest exchange through facilitated transport in a seemingly impenetrable hydrogen-bonded framework, J. Am. Chem. Soc. 140 (2018) 12915–12921;
e) I. Hisaki, Y. Suzuki, E. Gomez, B. Cohen, N. Tohnai, A. Douhal, Docking strategy to construct thermostable, single-crystalline, hydrogen-bonded organic framework with high surface area, Angew. Chem. Int. Ed. 57 (2018) 12650–12655;
f) Z. Bao, D. Xie, G. Chang, H. Wu, L. Li, W. Zhou, H. Wang, Z. Zhang, H. Xing, Q. Yang, M.J. Zaworotko, Q. Ren, B. Chen, Fine tuning and specific binding sites with a porous hydrogen-bonded metal-complex framework for gas selective separations, J. Am. Chem. Soc. 140 (2018) 4596–4603;
g) J. Mahmood, S.J. Kim, H.J. Noh, S.M. Jung, I. Ahmad, F. Li, J.M. Seo, J.B. Baek, A robust 3D cage-like ultramicroporous network structure with high gas-uptake capacity, Angew. Chem. Int. Ed. 57 (2018) 3415–3420;
h) Y.L. Wu, N. Bobbitt, J.L. Logsdon, N.E. Powers-Riggs, J.N. Nelson, X.L. Liu, T.C. Wang, R.Q. Snurr, J.T. Hupp, O.K. Farha, M.C. Hersam, M.R. Wasielewski, Tunable crystallinity and charge transfer in two-dimensional g-quadruplex organic frameworks, Angew. Chem. Int. Ed. 57 (2018) 3985–3989;
i) F.Q. Liu, J.W. Liu, Z. Gao, L. Wang, X.Z. Fu, L.X. Yang, Y. Tao, W.H. Yin, F. Luo, Constructing bimetal-complex based hydrogen-bonded framework for highly efficient electrocatalytic water splitting, Appl. Catal. B: Environ. 258 (2019) 117973–117980.

[7] a) Y. Cui, B. Li, H. He, W. Zhou, B. Chen, G. Qian, Metal-organic frameworks as platforms for functional materials, Acc. Chem. Res. 49 (2016) 483;
b) R.B. Lin, L. Li, H.L. Zhou, H. Wu, C. He, S. Li, R. Krishna, J. Li, W. Zhou, B. Chen, Molecular sieving of ethylene from ethane using a rigid metal-organic framework, Nat. Mater. 17 (2018) 1128–1133;
c) L. Li, R.B. Lin, R. Krishna, H. Li, S. Xiang, H. Wu, J. Li, W. Zhou, B. Chen, Ethane/ethylene separation in a metal-organic framework with iron-peroxo sites, Science 362 (2018) 443–446;
d) P.Q. Liao, N.Y. Huang, W.X. Zhang, J.P. Zhang, X.M. Chen, Controlling guest conformation for efficient purification of butadiene, Science 356 (2017) 1193–1196;
e) X. Cui, K. Chen, H. Xing, Q. Yang, R. Krishna, Z. Bao, H. Wu, W. Zhou, X. Dong, Y. Han, B. Li, Q.L. Ren, M.J. Zaworotko, B. Chen, Pore chemistry and size control in hybrid porous materials for acetylene capture from ethylene, Science 353 (2016) 141–144;
f) A. Cadiau, K. Adil, P.M. Bhatt, Y. Belmabkhout, M. Eddaoudi, A metal-organic framework-based splitter for separating propylene from propane, Science 353 (2016) 137–140;
g) Q. Gao, J. Xu, D. Cao, Z. Chang, X.H. Bu, A rigid nested metal-organic framework featuring a thermoresponsive gating effect dominated by counterions, Angew. Chem. Int. Ed. 55 (2016) 15027–15030;
h) Y.W. Li, H. Yan, T.L. Hu, H.Y. Ma, D.C. Li, S.N. Wang, Q.X. Yao, J.M. Dou, J. Xu, X.H. Bu, Two microporous Fe-based MOFs with multiple active sites for selective gas adsorption, Chem. Commun. 53 (2017) 2394–2397;
i) D.S. Zhang, Z. Chang, Y.F. Li, Z.Y. Jiang, Z.H. Xuan, Y.H. Zhang, J.R. Li, Q. Chen, T.L. Hu, X.H. Bu, Fluorous metal organic frameworks with enhanced stability and high H2/CO2 storage capacities, Scientific reports 3 (2013) 3312–3319;
j) Jerry Y.S. Lin, Molecular sieves for gas separation, Science 353 (2016) 121–122;
k) R.B. Lin, L. Li, H. Wu, H. Arman, B. Lin, R.G. Lin, W. Zhou, B. Chen, Optimized separation of acetylene from carbon dioxide and ethylene in a microporous material, J. Am. Chem. Soc. 139 (2017) 8022–8028.

[8] a) I. Hod, W. Bury, D.M. Gardner, P. Deria, V.V. Roznyatovskiy, M.R. Wasielewski, O.K. Farha, J.T. Hupp, Bias-switchable permselectivity and redox catalytic activity of a ferrocene-functionalized, thin-film metal-organic framework compound, J. Phys. Chem. Lett. 6 (2015) 586–591;
b) Y. Tulchinsky, C.H. Hendon, K.A. Lomachenko, E. Borfecchia, B.C. Melot, M.R. Hudson, J.D. Tarver, M.D. Korzyński, A.W. Stubbs, J.J. Kagan,

Carlo. Lamberti,-C.M.-Brown,-M.-Dincă, Reversible capture and release of Cl2 and Br 2 with a redox-active metal − organic framework, J. Am. Chem. Soc. 139 (2017) 5992–5997;
c) Q. Chen, J. Sun, P. Li, I. Hod, P.Z. Moghadam, Z.S. Kean, R.Q. Snurr, J.T. Hupp, O.K. Farha, J.F. Stoddart, A redox-active bistable molecular switch mounted inside a metal-organic framework, J. Am. Chem. Soc. 138 (2016) 14242–14245;
d) F.J. Claire, S.M. Tenney, M.M. Li, M.A. Siegler, J.S. Wagner, A.S. Hall, T.J. Kempa, Hierarchically ordered two-dimensional coordination polymers assembled from redox-active dimolybdenum clusters, J. Am. Chem. Soc. 140 (2018) 10673–10676;
e) B.A. Johnson, A. Bhunia, H. Fei, S.M. Cohen, S. Ott, Development of a Uio-type thin film electrocatalysis platform with redox-active linkers, J. Am. Chem. Soc. 140 (2018) 2985–2994;
f) L.X. Cai, S.C. Li, D.N. Yan, L.P. Zhou, F. Guo, Q.F. Sun, Water-soluble redox-active cage hosting polyoxometalates for selective desulfurization catalysis, J. Am. Chem. Soc. 140 (2018) 4869–4876;
g) D.M. D'Alessandro, Exploiting redox activity in metal-organic frameworks: concepts, trends and perspectives, Chem. Commun. 52 (2016) 8957–8971.

[9] a) S.V. Bhosale, C.H. Jani, S. Langford, Chemistry of naphthalene diimides, J. Chem. Soc. Rev. 37 (2008) 331–342;
b) B. Garai, A. Mallick, R. Banerjee, Photochromic metal-organic frameworks for inkless and erasable printing, Chem. Sci. 7 (2016) 2195–2200;
c) A. Mallick, B. Garai, M.A. Addicoat, P.S. Petkov, T. Heine, R. Banerjee, Solid state organic amine detection in a photochromic porous metal organic framework, Chem. Sci. 6 (2015) 1420–1425;
d) L. Han, L. Qin, L. Xu, Y. Zhou, J. Sun, X. Zou, A novel photochromic calcium-based metal-organic framework derive from a naphthalene diimide chromophore, Chem. Commun. 49 (2013) 406–408;
e) K. AlKaabi, C.R. Wade, M. Dincă, Transparent-to-dark electrochromic behavior in naphthalene-diimide-based mesoporous MOF-74 analogs, Chemistry 1 (2016) 264–272.

[10] A. Mallick, B. Garai, M.A. Addicoat, P.S. Petkov, T. Heine, R. Banerjee, Solid state organic amine detection in a photochromic porous metal organic framework, Chem. Sci. 6 (2015) 1420–1425.

[11] a) P. Li, Y. He, Y. Zhao, L. Weng, H. Wang, R. Krishna, H. Wu, W. Zhou, M.O. Keeffe, Y. Han, B. Chen, A rod-packing microporous hydrogen-bonded organic framework for highly selective separation of C2H2/CO2 at room temperature, Angew. Chem. Int. Ed. 54 (2015) 574–577;
b) J.P. Zhang, X.M. Chen, Optimized acetylene/carbon dioxide sorption in a dynamic porous crystal, J. Am. Chem. Soc. 131 (2009) 5516–5521;
c) F. Moreau, I.D. Silva, N.H. Al Smail, T.L. Easun, M. Savage, H.G.W. Godfrey, S.F. Parker, P. Manuel, S. Yang, M. Schröder, Unravelling exceptional acetylene and carbon dioxide adsorption within a tetra-amide functionalized metal-organic framework, Nat. Commun. 8 (2017) 14085–14093;
d) K.J. Chen, H.S. Scott, D.G. Madden, T.T. Pham, A. Kumar, A. Baipai, M. Lusi, K.A. Forrest, B. Space, J.J. Perry IV, M.J. Zaworotko, Benchmark C2H2/CO2 and CO2/C2H2 separation by two closely related hybrid ultramicroporous materials, Chemistry 1 (2016) 753–765;
e) M. Jiang, X. Cui, L. Yang, Q. Yang, Z. Zhang, Y. Yang, H. Xing, A thermostable anion-pillared metal-organic framework for C2H2/C2H4 and C2H2/CO2 separations, Chem. Eng. J. 352 (2018) 803–810;
f) Y. Belmabkhout, Z. Zhang, K. Adil, P.M. Bhatt, A. Cadiau, V. Solovyeva, H. Xing, M. Eddaoudi, Hydrocarbon recovery using ultra-microporous fluorinated MOF platform with and without uncoordinated metal sites: I-structure properties relationships for C2H2/C2H4 and CO2/C2H2 separation, Chem. Eng. J. 359 (2019) 32–36.

[12] a) F. Luo, C. Yan, L. Dang, R. Krishna, W. Zhou, H. Wu, X. Dong, Y. Han, T.L. Hu, M. O'Keeffe, L. Wang, M. Luo, R.B. Lin, B. Chen, A MOF-74 isomer with two accessible binding sites per metal center for highly selective gas separation, J. Am. Chem. Soc. 138 (2016) 5678–5684;
b) R. Krishna, Screening metal-organic frameworks for mixture separations in fixed-bed adsorbers using a combined selectivity/capacity metric, RSC Adv. 7 (2017) 35724–35737;
c) J. Lee, C.Y. Chuah, J. Kim, Y. Kim, N. Ko, Y. Seo, K. Kim, T.H. Bae, E. Lee, Separation of acetylene from carbon dioxide and ethylene by a water-stable microporous methal-organic framework with aligned imidazoliun groups inside the channels, Angew. Chem. Int. Ed. 57 (2018) 7869–7873.

[13] a) X. Li, T. Guo, L. Zhu, C. Ling, Q. Xue, W. Xing, Charge-odulated CO2 capture of C3N nanosheet: insights from DFT calculations, Chemical Engineering Journal 338 (2018) 92–98;
b) X. Li, Q. Xue, X. Chang, L. Zhu, H. Zheng, Fluorine-rich carbon nanoscrolls for CO2/CO(C2H2) adsorptive separation, J. CO2 Utilization 21 (2017) 429–435;
c) Z. Yao, Z. Zhang, L. Liu, Z. Li, W. Zhou, Y. Zhao, Y. Han, B. Chen, R. Krishna, S. Xiang, Extraordinary separation of acetylene-containing mixtures with microporous metal-organic frameworks with open O donor sites and tunable robustness through control of the helical chain secondary building unites, Chem. Eur. J. 22 (2016) 5676–5683.

[14] a) G. Xu, G.C. Guo, M.S. Wang, Z.J. Zhang, W.T. Chen, J.S. Huang, Photochromism of a methyl viologen bismuth (III) chloride: structural variation before and after UV irradiation, Angew. Chem. Int. Ed. 46 (2007) 3249–3251;
b) J.B. Wu, C.Y. Tao, Y. Li, Y. Yan, J.Y. Li, J.H. Yu, Methylviologen-templated layered bimetal phosphate: a multifunctional X-ray-induced photochromic material, Chem. Sci 5 (2014) 4237–4241;
c) R.G. Lin, G. Xu, G. Lu, M.S. Wang, P.X. Li, G.C. Guo, Photochromic Hybrid containing in situ-generated benzyl viologen and novel trinuclear $[Bi3Cl14]^{5-}$: improved photoresponsive behavior by the π···π interactions and size effect of inorganic oligomer, Inorg Chem. 53 (2014) 5538–5545.

Constructing redox-active microporous hydrogen-bonded organic framework by imide-functionalization: photochromism, electrochromism, and selective adsorption of C_2H_2 over CO_2

Li Wang[†a], Lixiao Yang[†a,] Lele Gong[†a], Rajamani Krishna[b], Zhi Gao[a], Yuan Tao[a], Wenhui Yin[a], Zhenzhen Xu[a], and Feng Luo[*a]

[a] State Key Laboratory of Nuclear Resources and Environment, School of Chemistry, Biology and Materials Science, East China University of Technology, Nanchang 330013, P. R. China

[b] Van‘t Hoff Institute for Molecular Sciences, University of Amsterdam, Science Park 904, 1098 XH Amsterdam, The Netherlands

[†] These authors contributed equally to this work

E-mail: ecitluofeng@163.com

1. Gas adsorption

1.1 Calculation of the separation potential of ECUT-HOF-30a

1.1.1 Fitting of unary isotherm data

The unary isotherm data for CO_2 and C_2H_2 measured at 273 K and 298 K in **ECUT-HOF-30a**, were fitted with the dual-site Langmuir-Freundlich model

$$q = q_{A,sat}\frac{b_A p^{\nu_A}}{1+b_A p^{\nu_A}} + q_{B,sat}\frac{b_B p^{\nu_B}}{1+b_B p^{\nu_B}} \tag{1}$$

with T-dependent parameters b_A, and b_B

$$b_A = b_{A0}\exp\left(\frac{E_A}{RT}\right); \quad b_B = b_{B0}\exp\left(\frac{E_B}{RT}\right) \tag{2}$$

1.1.2 Isosteric heat of adsorption

The isosteric heats of adsorption were calculated from the dual-site Langmuir-Freundlich model using

$$Q_{st} = RT^2\left(\frac{\partial \ln p}{\partial T}\right)_q \tag{3}$$

1.1.3 IAST calculations of component uptakes and selectivities

IAST calculations were performed for 50/50 C_2H_2/CO_2 mixtures at 298 K. The adsorption selectivity was calculated from

$$S_{ads} = \frac{q_A/q_B}{y_A/y_B} \tag{4}$$

where the q_A, and q_B represent the molar loadings in ECUT-HOF-30 that is in equilibrium with a bulk fluid mixture with mole fractions y_A, and y_B = 1 - y_A. The molar loadings, also called *gravimetric uptake capacities*, are expressed in mol kg^{-1}. The IAST calculations for the mixtures were performed at 298 K, taking the mole fractions y_A = 0.5 and y_B = 1 - y_A = 0.5.

1.1.4 Transient breakthrough of mixtures in fixed bed adsorbers

The performance of industrial fixed bed adsorbers is dictated by a combination of adsorption selectivity and uptake capacity. Transient breakthrough simulations were carried out for 50/50 C_2H_2/CO_2 mixtures operating at a total pressure of 100 kPa and 298 K, using the methodology

described in earlier publications *(Microporous Mesoporous Mater.* ***2014****, 185, 30, RSC Adv.* ***2015****, 5, 52269, R. RSC Adv.* ***2017****, 7, 35724, Sep. Purif. Technol.* ***2018****, 194, 281)*. For the breakthrough simulations, the following parameter values were used: length of packed bed, L = 0.3 m; voidage of packed bed, □= 0.4; superficial gas velocity at inlet, u = 0.04 m/s. The transient breakthrough simulation results are presented in terms of a *dimensionless* time, $\tau = \frac{tu}{L\varepsilon}$. The y-axis is dimensionless concentration at the exit of the fixed bed asdsorber, $\frac{c_i}{c_{i0}}$.

Nomenclature

Latin alphabet

b	Langmuir-Freundlich constant, $\mathrm{Pa}^{-\nu}$
p_i	partial pressure of species i in mixture, Pa
q_i	component molar loading of species i, mol kg^{-1}
q_A	gravimetric uptake of species A, mol kg^{-1}
q_sat	saturation loading, mol kg^{-1}
L	length of packed bed adsorber, m
t	time, s
T	absolute temperature, K
u	superficial gas velocity in packed bed, m s^{-1}
y_A	gas phase mole fraction of species A, dimensionless
y_B	gas phase mole fraction of species B, dimensionless

Greek letters

□	voidage of packed bed, dimensionless
□$_\mathrm{i}$	molar chemical potential, J mol^{-1}
□	Exponent in Langmuir-Freundlich isotherm model, dimensionless
□	framework density, kg m^{-3}
□	time, dimensionless

Subscripts

i,j	components in mixture
i	referring to component i
t	referring to total mixture
sat	referring to saturation conditions

Table S1. A comparison of HOFs with their aperture.

Compounds	Pore size (Å)	Reference
HOF-1a	8.2	*J. Am. Chem. Soc.*, **2011**, 133, 14570
HOF-2	4.8	*J. Am. Chem. Soc*. **2014**,136,547
HOF-3a	7.0	*Angew. Chem. Int. Ed.*, **2015**, 54, 574
HOF-4	3.8×8.1	*Chem.commun.* **2014**, 50, 13081
HOF-5	4.0×6.8 along [-101] 3.9×5.4 along [001] 4.1×6.8 along [001]	*J. Am. Chem. Soc.* **2015,** 137, 9963
HOF-5a	3.9×6.8 along [001] 3.9×5.5 along [100]	*J. Am. Chem. Soc.* **2015,** 137, 9963
HOF-6	6.4 along [101] 7.5 along [100]	*Cryst. Growth Des.* **2016**,16,5831
HOF-7	3.2×4.7 4.2×6.7	*Cryst. Growth Des.* **2015**,15,2000
HOF-8	6.8×4.5	*J. Am. Chem. Soc.***2013**,135,11684
HOF-10	12.8×26.0 3.2*4.7, 4.2*6.7	*Chem. Comm.* **2017**,53,11150
HOF-11	6.2×6.8	*Crystal Growth & Design* **2017**,17,6132
H_cOF-1	15.0×10.4 7.3×5.5 along [100] 7.3×6.3 along [101]	*J. Am. Chem. Soc.* **2017**,139, 7172
HOF-TPE3N	7.655×7.655	*Chem. Sci.* **2017**, 8, 1163
HOF-TPE4N	5.855×5.855 (α cage) 7.218×7.218 (β cage)	*Chem. Sci.* **2017**, 8, 1163
HOF-TCPP-1,3-DPP	20×18	*Adv. Funct. Mater.* **2018**, 180,4822
HOF-1111	6.8×10.9	*Cryst. Growth Des.* **2015**,15,542
CPHAT-1-(TCB)	6.7×8.8	*Chem. Eur. J.* **2017**, 23, 11611
HOF based trispyrazole	16.5	*Nat. Commun.* **2014**, 5, 1
SOF-7a	13.5×14	*J. Am. Chem. Soc.* **2014**, 136, 12828.
HOF-PFC-1	18×23	*Angew. Chem. Int. Ed.* **2018**, 130, 7817
HOF-21	3.6	*J. Am. Chem. Soc.***2018**, 140, 4596
PFC-1	18×23	*Angewandte Chemie* **2018**, 130, 7817
CBPHAT-1(TCB)	14.5	*Angew. Chem. Int. Ed.***2018**, 57, 12650
T-SOF_{-1}	6.3, 4.5	*J. Am. Chem. Soc.* **2018**, 140, 14571
ECUT-HOF-30	**4.0×4.1**	**This work**

Table S2. A comparison of C_2H_2/CO_2 uptake ratio at 298K (or 296K) and 1 bar among HOFs and selected MOFs.

Compounds	$V(CO_2)$ $[cm^3g^{-1}]$	$V(C_2H_2)$ $[cm^3g^{-1}]$	Adsorption ratio (C_2H_2/CO_2)	References
ECUT-HOF-30	9.0	44.5	**4.94**	**This work**
SOF-1a	16	50	3.13	*J. Am. Chem. Soc.* **2010**,132,14457
HOF-3a	21	47	2.24	*Angew. Chem. Int. Ed.*, **2015**, 54, 574
HOF-5a	90	102	1.13	*J. Am. Chem. Soc.* **2015**,137,9963
HOF-11	30	45	1.5	*Crystal Growth & Design* **2017**,17,6132
UTSA-74	71	110	1.5	*J. Am. Chem. Soc.* **2016**, 138, 5678
BUT-70A	19.3	69.5	3.6	*Inorg.Chem.***2017**,56,2188
BUT-70B	31.3	87.1	2.78	*Inorg.Chem.***2017**,56,2188
FJU-22a	111.3	114.8	1.03	*Chem.Eur.J.***2016**,22,5676
JCM-1	38	75	1.97	*Angew. Chem. Int. Ed.* **2018**, 57,7869
MAF-2	19	70	3.68	*J. Am. Chem. Soc.* **2009**,131, 5516
ZJU-199a	62.4	128	2.05	*Cryst.Growth Des.***2016**,16,7194
UTSA-300a	4	68	17	*J. Am. Chem. Soc.* **2017**, 139, 8022
Co-MOF	60	145	2.41	*Inorg.Chem.***2017**,56,14767
DICRO-4-Ni-i	23	43	1.87	*Appl.Mater.Interfaces.***2016**,9,33395
MFM-188a	120	232	1.93	*Nat. Commun.* **2017**, 8, 14085
SIFSIX-3-Ni	60.5	73.9	1.22	*Chem.* **2016**, 1, 753.
TIFSIX-2-Cu-i	96.3	118.7	1.23	*Chem.* **2016,** 1, 753
TIFSIX-2-Ni-i	101.7	94.3	0.93	*Chemical Engineering Journal* **2018**,352,803
AIFFIVE-1-Ni	62.7	100.8	1.6	*Chemical Engineering Journal* **2019**,359,32
NbOFFIVE-1-Ni	49.28	53.76	1.09	*Chemical Engineering Journal* **2019**,359,32

2. Characterizations

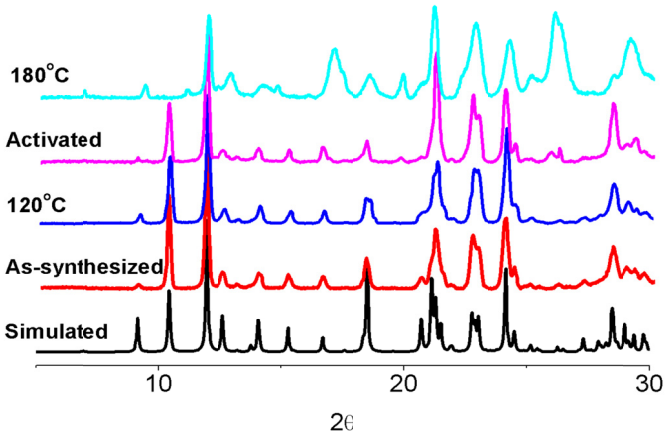

Figure S1. The PXRD patterns of **ECUT-HOF-30** at different temperatures, as-synthesized samples, the activated samples, and the PXRD patterns simulated from single crystal data.

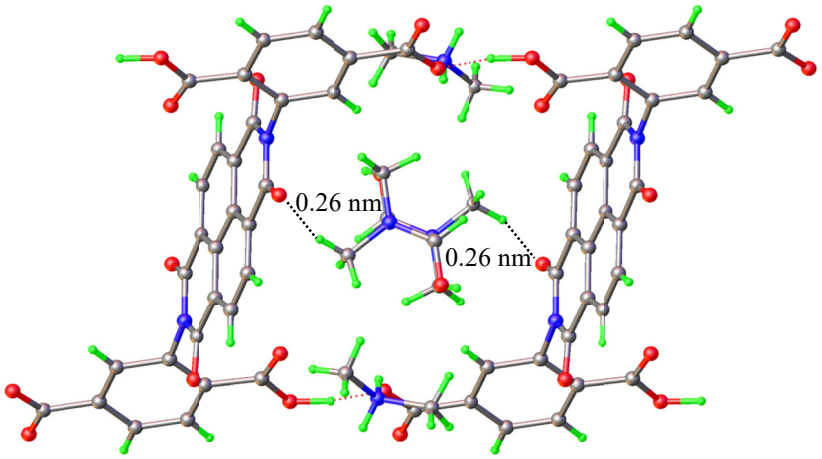

Figure S2. View of the very weak C-H…O supramolecular interactions between DMF molecules and HOF framework.

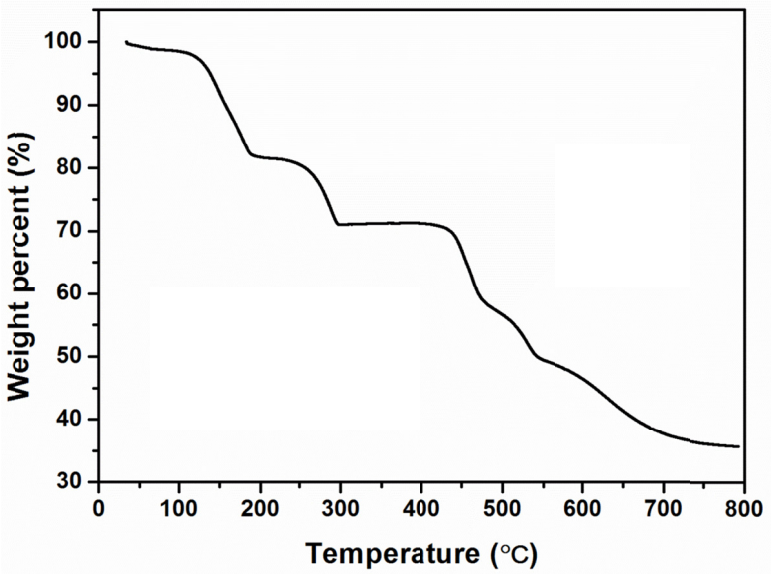

Figure S3. TGA curve of **ECUT-HOF-30** in the range of 25-800^{o}C under N_2 atmosphere.

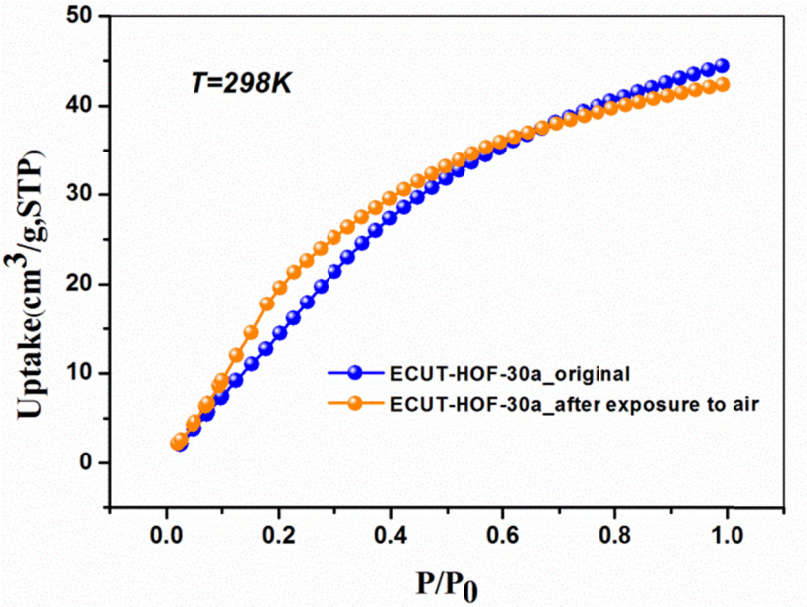

Figure S4: The C_2H_2 adsorption of **ECUT-HOF-30a** before and after exposure to air

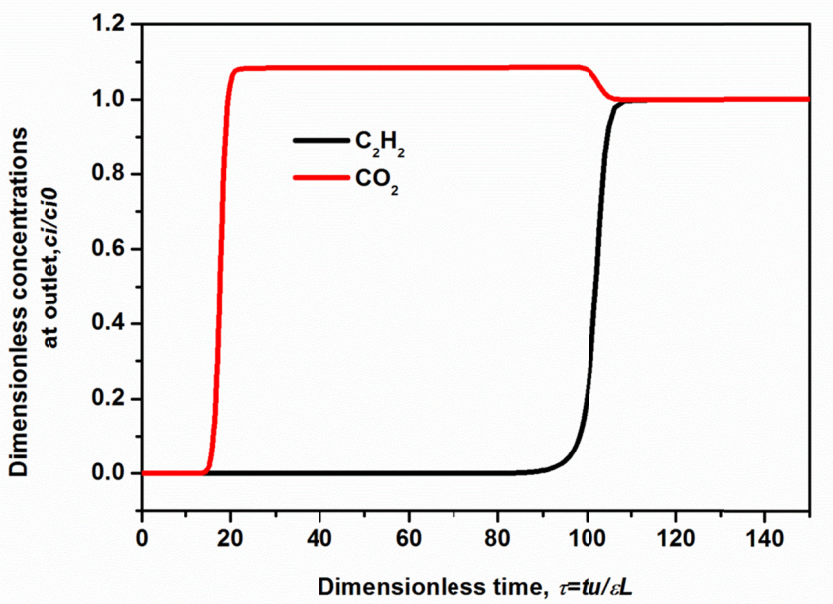

Figure S5. Transient breakthrough simulations for separation of equimolar C_2H_2/CO_2 mixture with partial pressures of 50 KPa at 298 K.

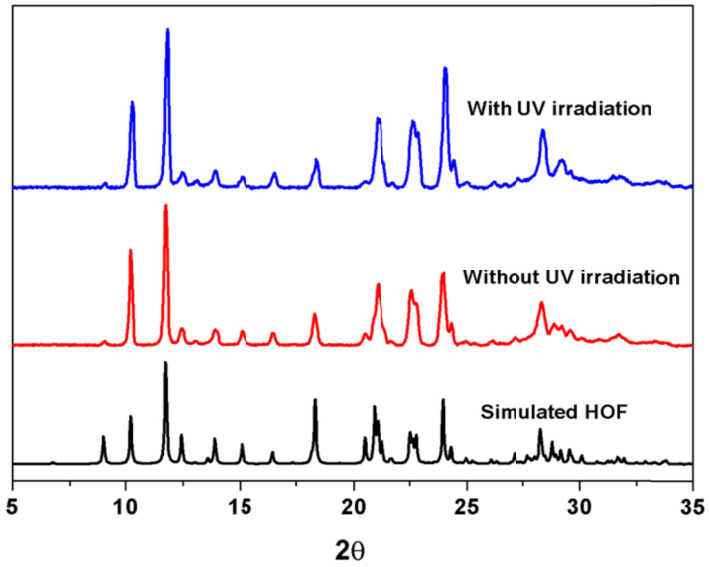

Figure S6. PXRD patterns of **ECUT-HOF-30** samples with and without UV irradiation (365 nm).

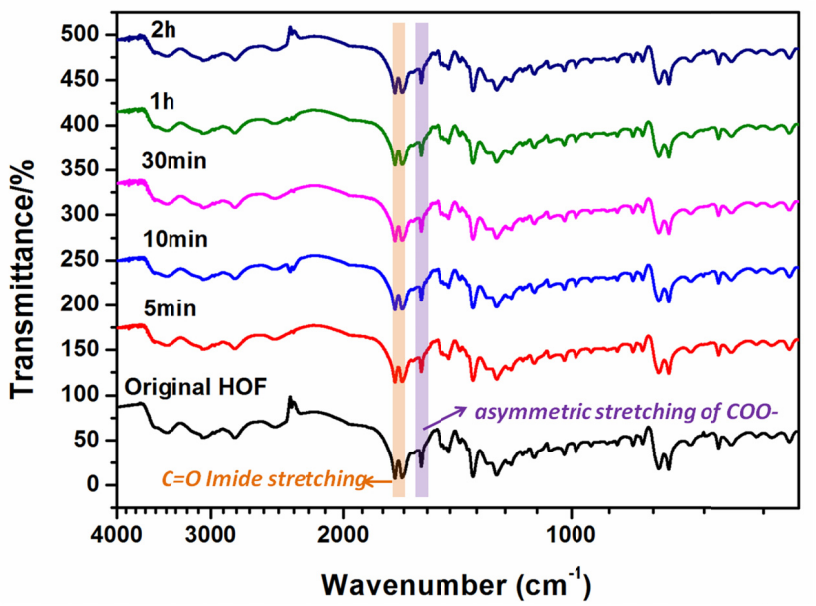

Figure S7. Time-dependent FT-IR spectra of **ECUT-HOF-30** upon UV irradiation (365 nm).

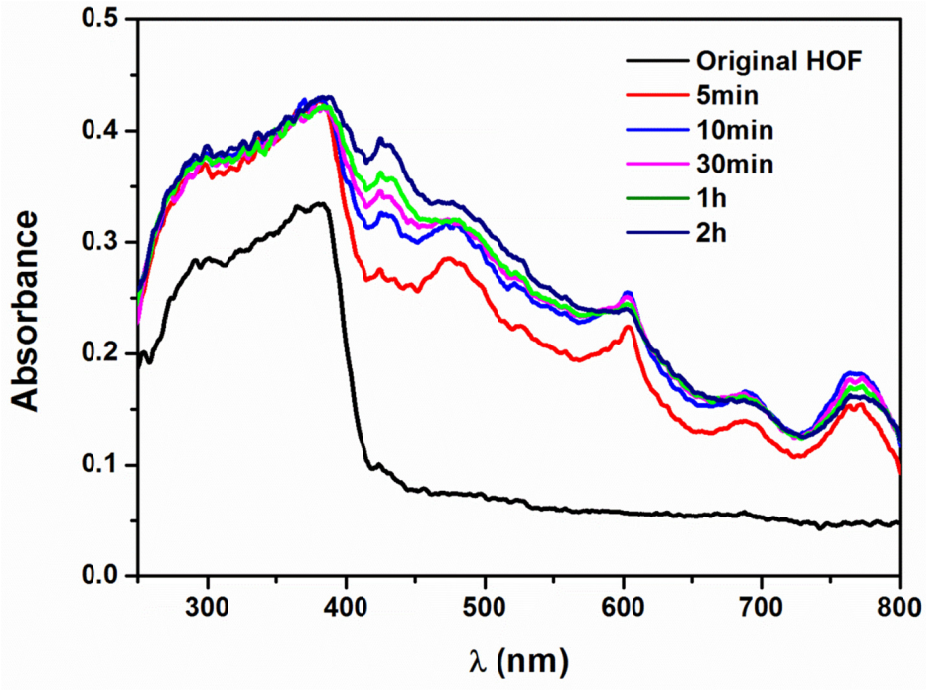

Figure S8. Time-dependent UV-Vis spectra of **ECUT-HOF-30** upon UV irradiation (365 nm).

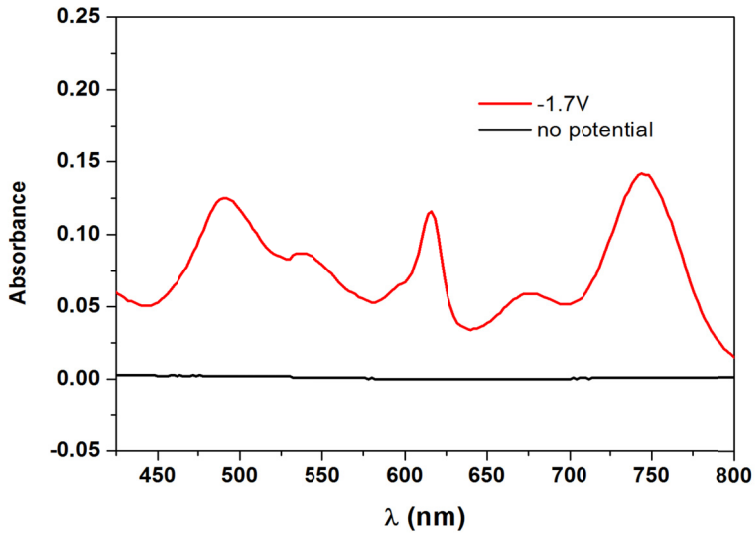

Figure S9. The in-situ UV-Vis spectra of **ECUT-HOF-30** without potential or with -1.7 V potential.